Continuum Methods II

John Lowengrub
Dept Math
UC Irvine

Microfluidics

Microscopic drop formation and manipulation:

- DNA analysis,
- Analysis of human physiological fluids
- Protein crystalization

Droplets used to improve mixing efficiency

- Coalescence,
- Inter-drop mixing

Channel geometry is used to control hydrodynamic forces

Tan et al, Lab Chip 2004

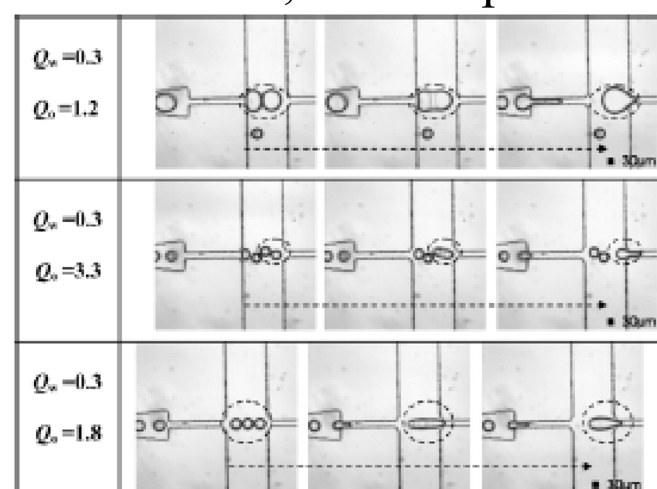

Fig. 3 Fusion of large droplet slugs and free flowing droplets is controlled by the external flow, which changes depending on the geometry and surface properties of the walls (data from ref. 10). Flow rates are in μl min^{-1}.

Muradoglu, Stone PF 2005

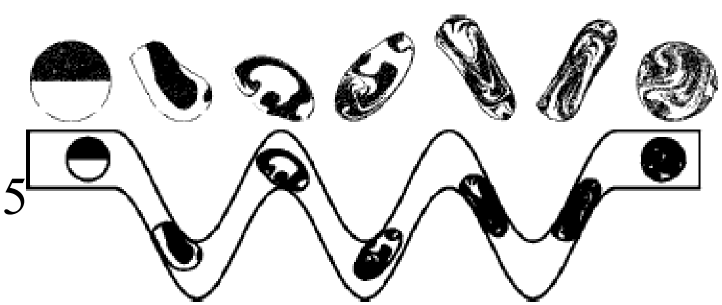

FIG. 3. Snapshots of mixing patterns taken at the nondimensional times from left to right $t^*=0$, 0.42, 0.90, 2.32, 1.80, 2.22 and 2.64, respectively. The top plots are the enlarged versions of the corresponding scatter plots shown in the channel (bottom plots). ($Ca=0.025, Re=6.6, \lambda=1.0, \Lambda=0.76$, Grid: 1024×64.)

Typical flows

- Stokes/Navier-Stokes equations
- Complex geometry
- Topology changes (pinchoff/reconnection)
- Multiple fluids

- In this talk, will focus on techniques for solving such problems on larger scales that have application to microfluidics
  - Drop/Interface interactions
  - Coalescence cascades in polymer blends

Motivation and Physical Application

Drop/Interface Impact

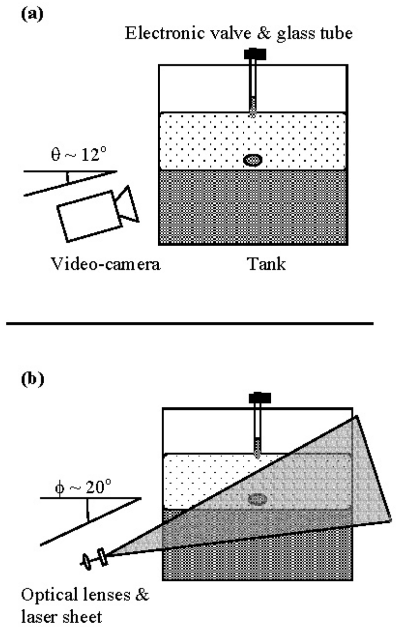

Z. Mohammed-Kassim,

E. K. Longmire Phys Fluids, 2003

- Many engineering, industrial, and biomedical applications

- Fundamental study of topological changes

- Very difficult test for numerical methods (need to resolve near contact region accurately)

Experiments: Drop/Interface Impact and Coalescence

Z. Mohammed-Kassim, E. K. Longmire Phys Fluids, 2003

Characterized by:

$$\lambda, \;\; \rho_d / \rho_a, \; \mathrm{Re}, \; We, Fr$$

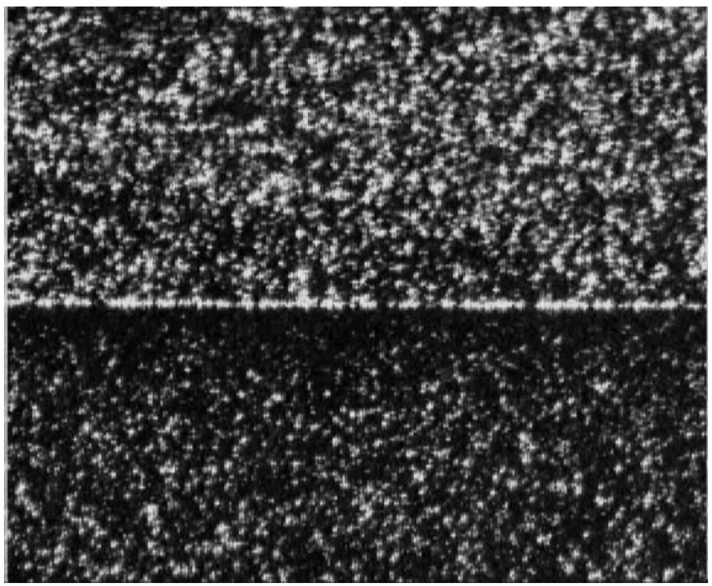

Water/glycerin Drop
oil ambient

Water/glycerin

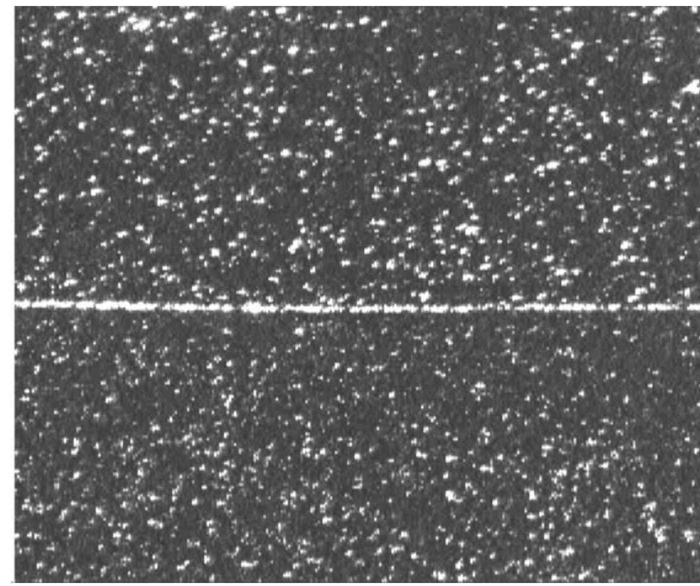

- Slow gap drainage
- Rebound of drop
- 3D initiation of coalescence

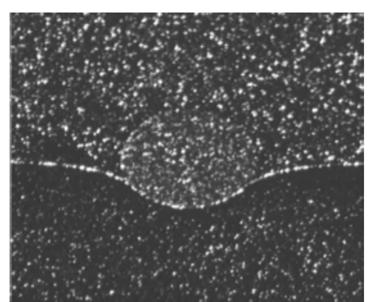

- Dependence on viscosity of outer fluid

Mathematical Model

Multiphase Navier-Stokes System

$$\left(\frac{\partial \mathbf{u}}{\partial t} + \mathbf{u} \bullet \nabla \mathbf{u}\right) = \nabla \bullet \mathbf{T} - \frac{1}{\mathrm{Fr}}(\rho - 1)\mathbf{g}$$

Boussinesq

$$\nabla \bullet \mathbf{u} = 0$$

$$\mathbf{T} = -pI + \frac{\mu}{\mathrm{Re}}\left(\nabla \mathbf{u} + \nabla \mathbf{u}^T\right)$$

$$[\mathbf{Tn}]_\Sigma = -\frac{1}{\mathrm{We}}\kappa \mathbf{n}, \quad [\mathbf{u}]_\Sigma = \mathbf{0}$$

$$\mathbf{n} \bullet \frac{d\mathbf{x}_\Sigma}{dt} = \mathbf{u} \bullet \mathbf{n}$$

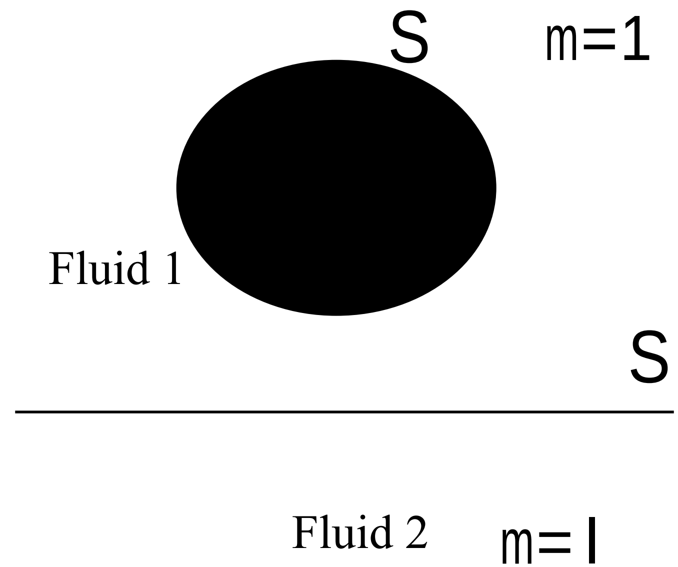

- Highly nonlinear, non-local free boundary problem

Numerical methods for Multiphase Flows

- Boundary Integral Method: highly accurate, difficult to perform topological changes, limited physics
- Mesh-Free Methods such as Particle methods: Marker Point method, Molecular Dynamics, Dissipative Particle Dynamics
- Diffuse Interface Methods: physically based, popular in material science
- Front Tracking Methods:: sharp interface, accurate hard to do topology changes
- Volume of Fluid Method (VOF): automatic topological changes, difficult to reconstruct interfaces. Conservation of mass
- Level-set Method: automatic topological changes, easy to compute interface geometry, loss of mass

Trends in Numerical Methods:

- Hybrid method: combining the advantages of existing methods, for example, combined LS and VOF, combined MP and VOF, etc

- Adaptive Mesh: moving mesh, locally refined mesh, etc

Difficulty in simulating drop/interface impact

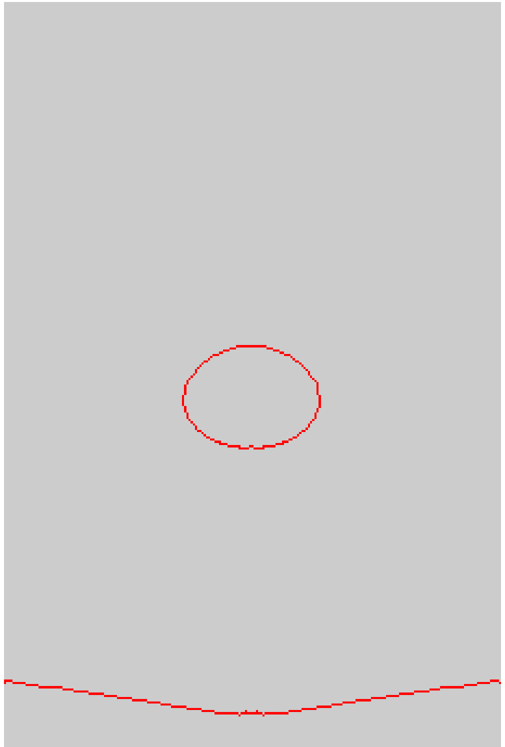

Uniform mesh

This structured mesh has 14400 nodes. Almost the same number of nodes as in our adaptive mesh simulation.

- Accurate evolution on large scale
- Inaccurate in near-contact region
- Unphysical coalescence
- Expensive to resolve near-contact region using uniform mesh

→ Adaptive Mesh Refinement

Adaptive Mesh Refinement/ Multiphase Navier-Stokes Equations/ Finite-element/ Level-set/ Method

Anderson, Zheng, Cristini. J. Comp. Phys. (2005)

Zheng, Lowengrub, Anderson, Cristini. J. Comp. Phys. (2005)

Adaptive mesh refinement

•Unstructured meshes (our work)

-Triangles (2-D, Axisymmetric)

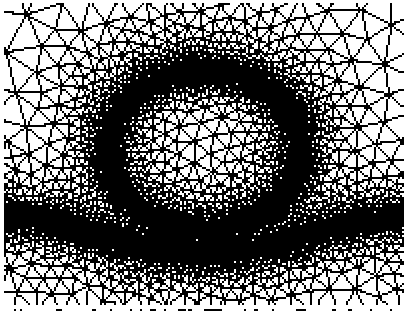

-Tetrahedra (3-D)

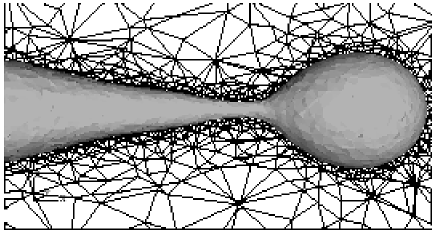

(Other 2D unstructured mesh work:
Ubbink and Issa 1999;
Ginzberg and Wittum 2001)

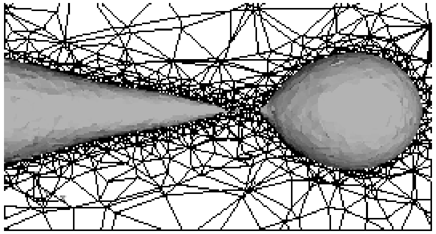

Other approaches:

•Mesh mapping/moving meshes

(Huang et al, Ren and Wang, Hou and Ceniceros, Wilkes et al…)

•Structured mesh refinement

(Provatas et al, Sussman et al, Ceniceros and Roma, Agresar et al.,…)

Adaptive Mesh Refinement Contd.

Anderson, Zheng, Cristini J. Comp. Phys. (2005)
Cristini et al. J. Comp. Phys. 2001

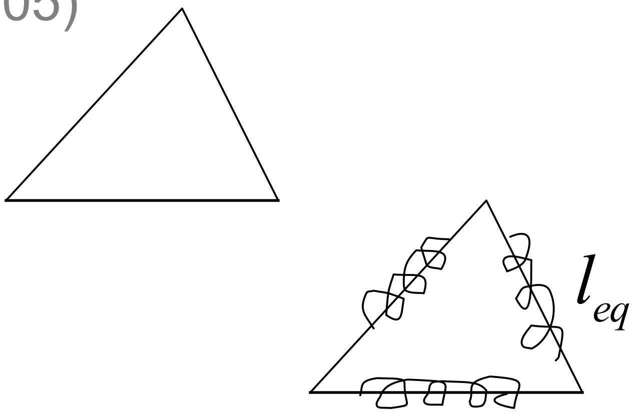

• Regard mesh edges as damped springs, define local equilibrium length scale according to relevant physical quantities

• Mesh energy function

Optimal mesh $\Leftrightarrow$ Global minimum of E

Local operations

- Equilibration
- Node reconnection
- Node addition/subtraction

Adaptive Mesh Refinement: Axisymmetric Domain

- Embed axisymmetric domain(red box) in a square domain where the mesh is refined
- Align the mesh to the axisymmetric boundary(red lines).

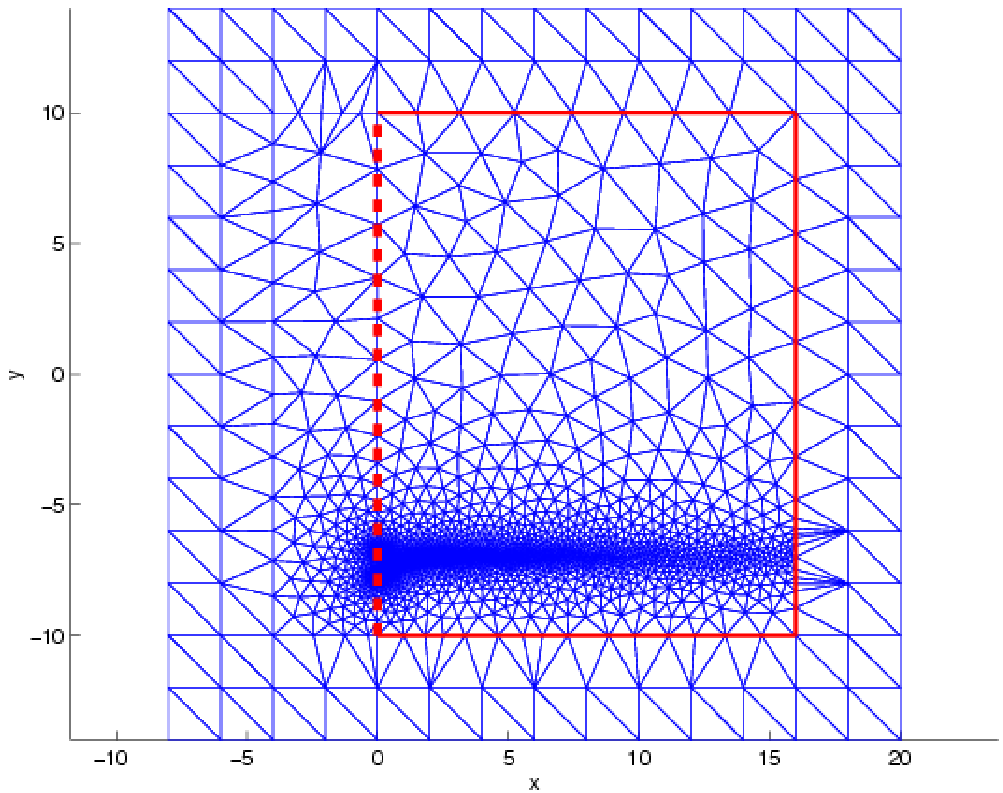

•Algorithm can be used for complex boundaries

Zheng, Lowengrub, Cristini. In preparation.

Alignment to axis of symmetry

1. First we select all the edges that intersect with the axis, and from the two endpoints of each such edge, we select the one closer to the axis to be the candidate to project to the axis. After we collect all the candidates as subset S1.
2. Then we check every triangle, if all its vertices are in S1, then we delete its node farthest from the axis from S1. After checking all triangles, we get subset S2. We project all nodes in S2 to the axis orthogonally.
3. After step 2, some intersecting edges would have no endpoints projected, then we add the crossing points of such edges with the axis into the mesh, with two additional edges added.

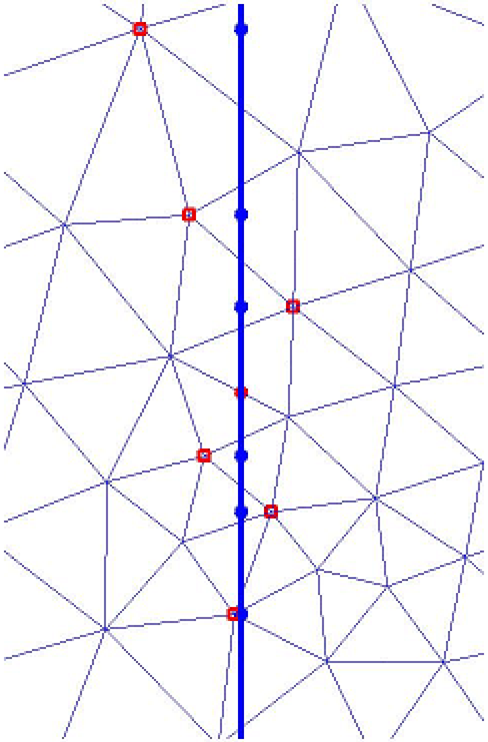

Before alignment

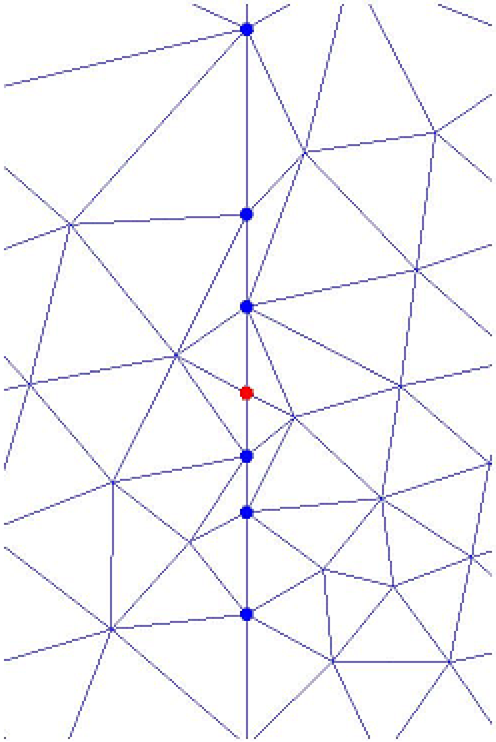

After alignment

ε

Distribution Boussinesq Navier-Stokes equations

$$\left(\frac{\partial \mathbf{u}}{\partial t} + \mathbf{u} \bullet \nabla \mathbf{u}\right) = \nabla \bullet \mathbf{T} - \frac{1}{\mathrm{Fr}}(\rho - 1)\mathbf{g}$$

$$\nabla \bullet \mathbf{u} = 0$$

$$\mathbf{T} = -pI + \frac{\mu}{\mathrm{Re}}\left(\nabla \mathbf{u} + \nabla \mathbf{u}^T\right) + \frac{1}{\mathrm{We}}\left(I - \mathbf{nn}\right)\delta_\Sigma$$

Singular surface stress (Zaleski et al.)

Interface(Level-set representation): (Osher-Sethian, Sussman…)

$$\Sigma = \left\{\mathbf{x} \,|\, \phi(\mathbf{x}, t) = 0\right\}, \qquad \mathbf{n} = \nabla\phi / |\nabla\phi|, \qquad \delta_\Sigma = \delta(\phi)\,|\nabla\phi|$$

$$\rho = 1 + (\rho_d / \rho_a - 1)\chi \qquad \mu = 1 + (\lambda - 1)\chi$$

$\varepsilon = O(h^\alpha), \alpha < 1$

Level-set evolution: $\dfrac{\partial\phi}{\partial t} + \mathbf{u} \bullet \nabla\phi = 0$

Level-set re-initialization:

$$\frac{\partial d}{\partial \tau} - \mathrm{sgn}(\phi)(1 - |\nabla d|) = 0, \;\; d(\mathbf{x}, \tau = 0) = \phi(\mathbf{x}, t)$$

Uzawa-Projection Method For NSE

- Navier-Stokes Eqns: $$\frac{\partial \boldsymbol{u}}{\partial \boldsymbol{t}} + (\boldsymbol{u} \bullet \nabla)\boldsymbol{u} + \nabla p = \frac{1}{\mathrm{Re}} \nabla^2 \boldsymbol{u} + \boldsymbol{f}$$
$$\nabla \bullet \boldsymbol{u} \qquad = 0$$

- Uzawa Projection scheme: use iteration to improve accuracy

$$\frac{\boldsymbol{u}^{*,l+1} - \boldsymbol{u}^{n}}{\Delta t} + (\boldsymbol{u} \bullet \nabla \boldsymbol{u})^{n+1/2,l} + \nabla p^{n+1/2,l} = \frac{1}{\mathrm{Re}} \frac{\nabla^2 \boldsymbol{u}^{*,l+1} + \nabla^2 \boldsymbol{u}^{n}}{2} + \boldsymbol{f}^{n+1/2},$$

$$\boldsymbol{u}^{*,l+1} = \boldsymbol{u}^{n+1,l+1} + \Delta t \nabla q^{n+1,l+1}, \qquad \nabla \bullet \boldsymbol{u}^{n+1,l+1} = 0,$$

$$p^{n+1/2} = p^{n-1/2} + q^{n+1,l+1} - \frac{\Delta t}{\mathrm{Re}} \Delta q^{n+1,l+1},$$

$$\boldsymbol{u}^{n+1/2,0} = \boldsymbol{u}^{n}, \qquad p^{n+1/2,0} = p^{n-1/2}$$

- Advantages:
  1. Improve accuracy for nonlinear terms;
  2. Improve incompressibility of velocity, especially with singular force;
  3. In adaptive mesh refinement, only need information from one earlier time step.

Implementation of FE/LS Adaptive Method

Zheng, Lowengrub, Anderson, Cristini, J. Comp. Phys. (2005)

- *Navier-Stokes Eqns* with variable density and viscosity

  Mixed Finite Element Uzawa-Projection method(P2/P1, MINI)

- *Level set*: Discontinuous Galerkin Method(TVD_RK2, P1)

- *Surface tension term:*

  we use capillary tensor, $(I-\boldsymbol{nn})\delta_\Sigma$ smoothing
  only normal is needed
  (integration by parts),
  which is easy to compute

- *Reinitialization*: Explicit Positive Coefficient Scheme

  (Barth and Sethian, 1998)

- *Adaptive mesh*: $l_{eq}(\mathbf{x}) \approx dist(\mathbf{x}, \Sigma)$

$$= \min(h_0, h + s\,|\,\phi(\mathbf{x}, t)\,|)$$

Efficiency of FE/LS Adaptive Method

h = smallest mesh size,
then d.o.f.(N)=O(1/h^(n-1)) in adaptive mesh, compared to O(1/h^n) in uniform n-dimensional mesh.

$N^{5/4}/h$ in 2D

$N^{7/6}/h$ in 3D

Evolution Solver Cost (FEM is based MINI elements)

Method	2D	3D
Adaptive FEM	h^(-2.25)	h^(-3.33)
Non-adaptive FEM	h^(-3.5)	h^(-4.5)
Boundary Integral	h^(-3)	h^(-5)

- Remeshing cost: $O(h^{-(n-1)})$ → very small compared to flow solver
- Example: gap $h \sim 10^{-3}$

→ 6,000-fold reduction in CPU time

Application to drop interface impact

Axisymmetric results

$\lambda = 0.33,\ \rho_d / \rho_a = 1.19,\ \mathrm{Re} = 68,\ \mathrm{We} = 7,\ \mathrm{Fr} = 1$

Experiment Simulation

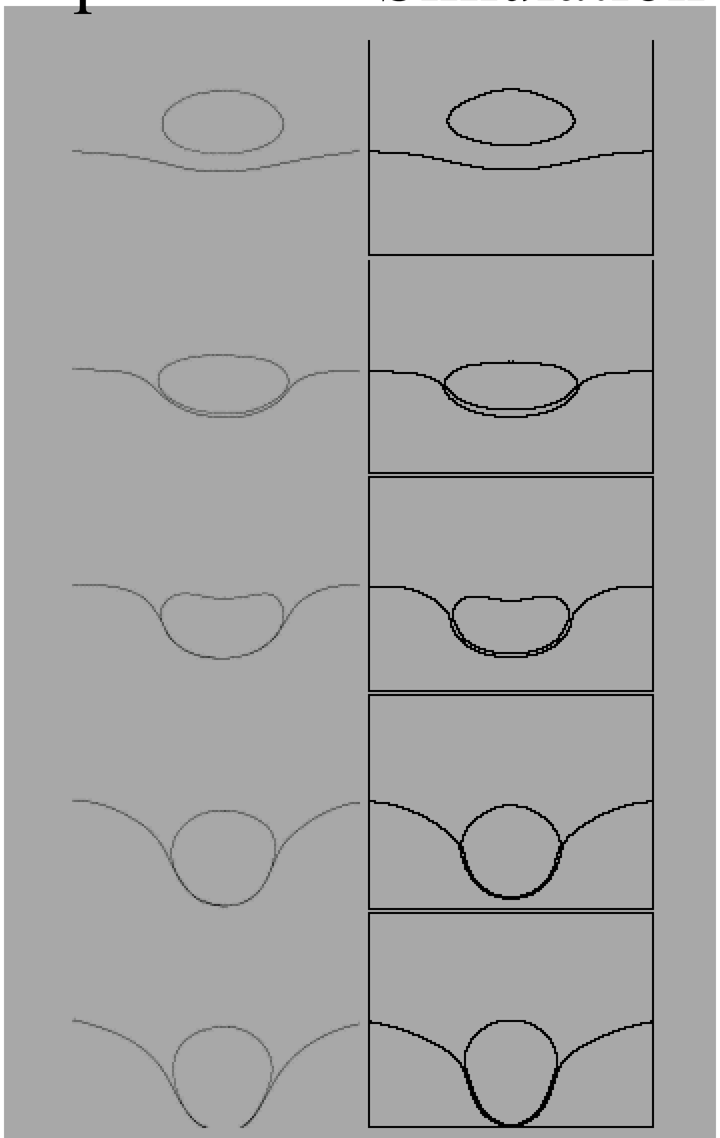

t=0

t=0.5

t=0.9

t=1.4

t=1.8

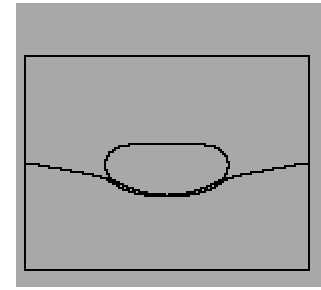

t=5

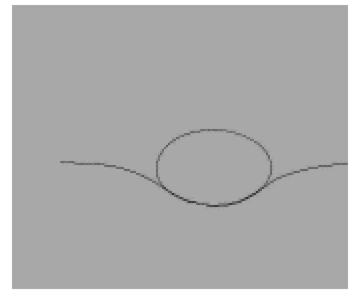

t=7

- Excellent agreement with experiment

Axisymmetric simulation

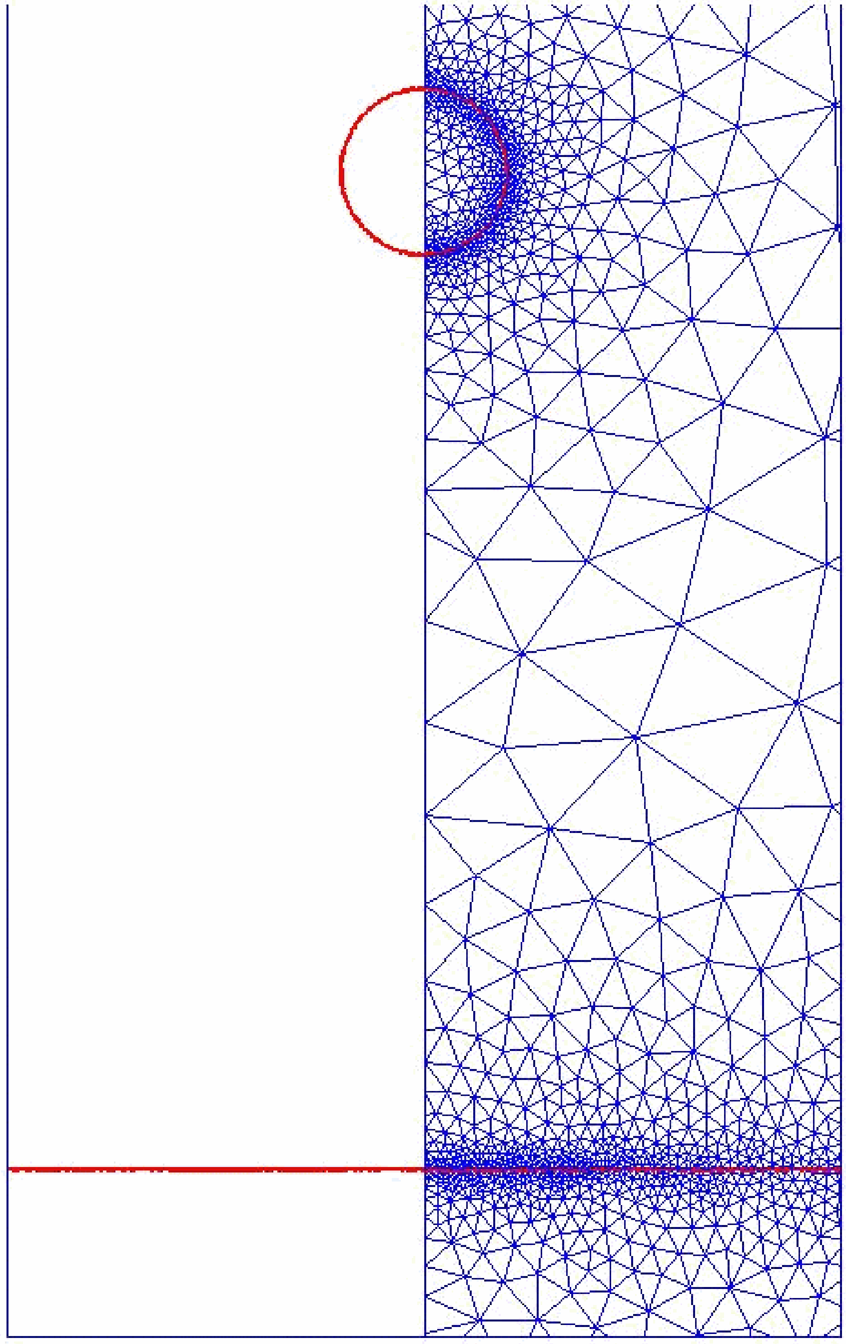

- Adaptive mesh follows interface
- Near contact regions accurately resolved
- Drop rebound is captured

The adaptive mesh

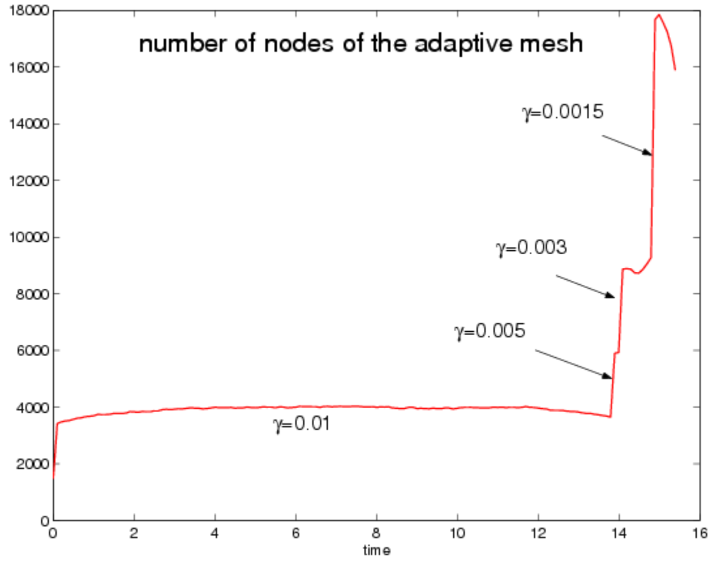

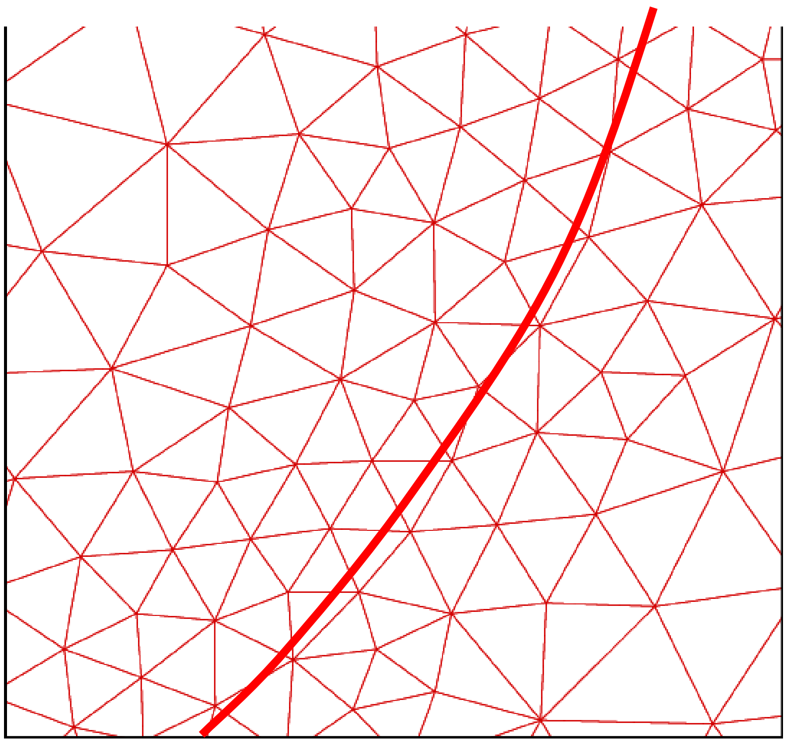

Largest mesh size
=2,
Smallest mesh size
=0.002

10 times zoom-in of each boxed region.

There are total 15890 nodes in the axisymmetric domain

Quantative comparison with experiment

Normalized location of interface and drop surface

- Solid lines are from numerical simulations
- Symbols are from experiments

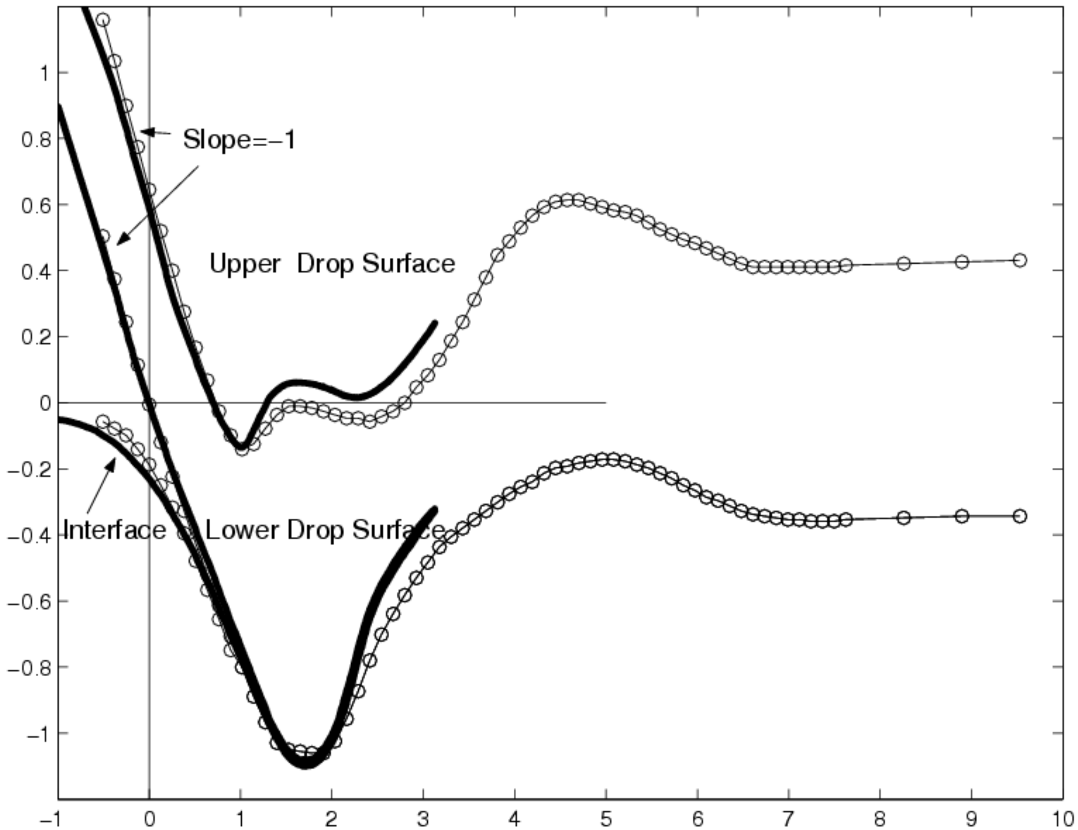

Comparison to non-adaptive mesh

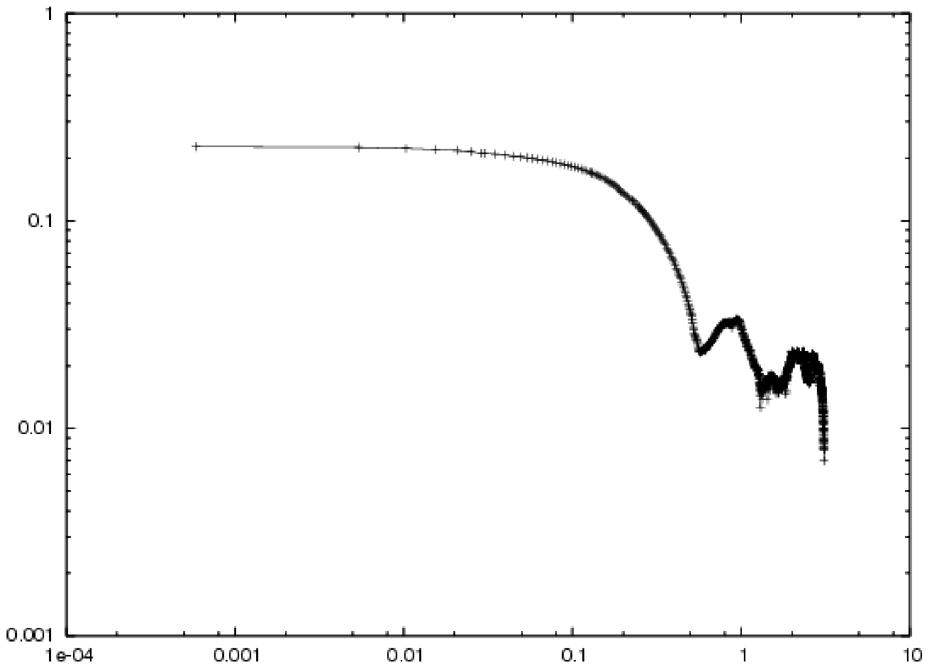

Minimum distance between drop and interface is 0.007, smallest mesh size h=0.002, effectively 3.6E+7 nodes in uniform mesh.

Extensions

- Hybrid methods

Adaptive Level-Set Volume-of-Fluid (ACLSVOF)

Yang, James, Lowengrub, Zheng, Cristini JCP 2006

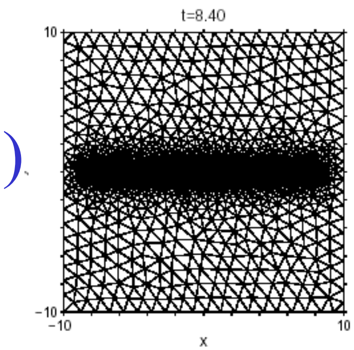

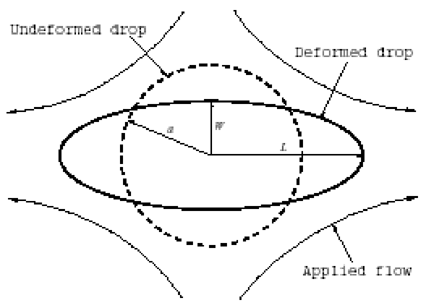

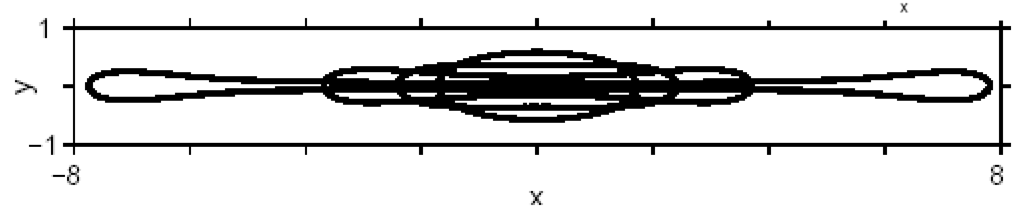

- Complex fluids

Viscoelastic flows-- Pillapakkam and Singh, JCP 2001

Surfactants– Xu, Li, Lowengrub, Zhao JCP 2006

Multi-drop simulation with surfactant

Xu, Li, Lowengrub, Zhao JCP 2006

Ca=0.7, Pe=10, E=0.2, x=0.3, f(.,0)=1. $\Omega=[-9,9]\times[-5,5], h=0.01, \Delta t = h/8$

Complex drop morphologies and surfactant distributions.

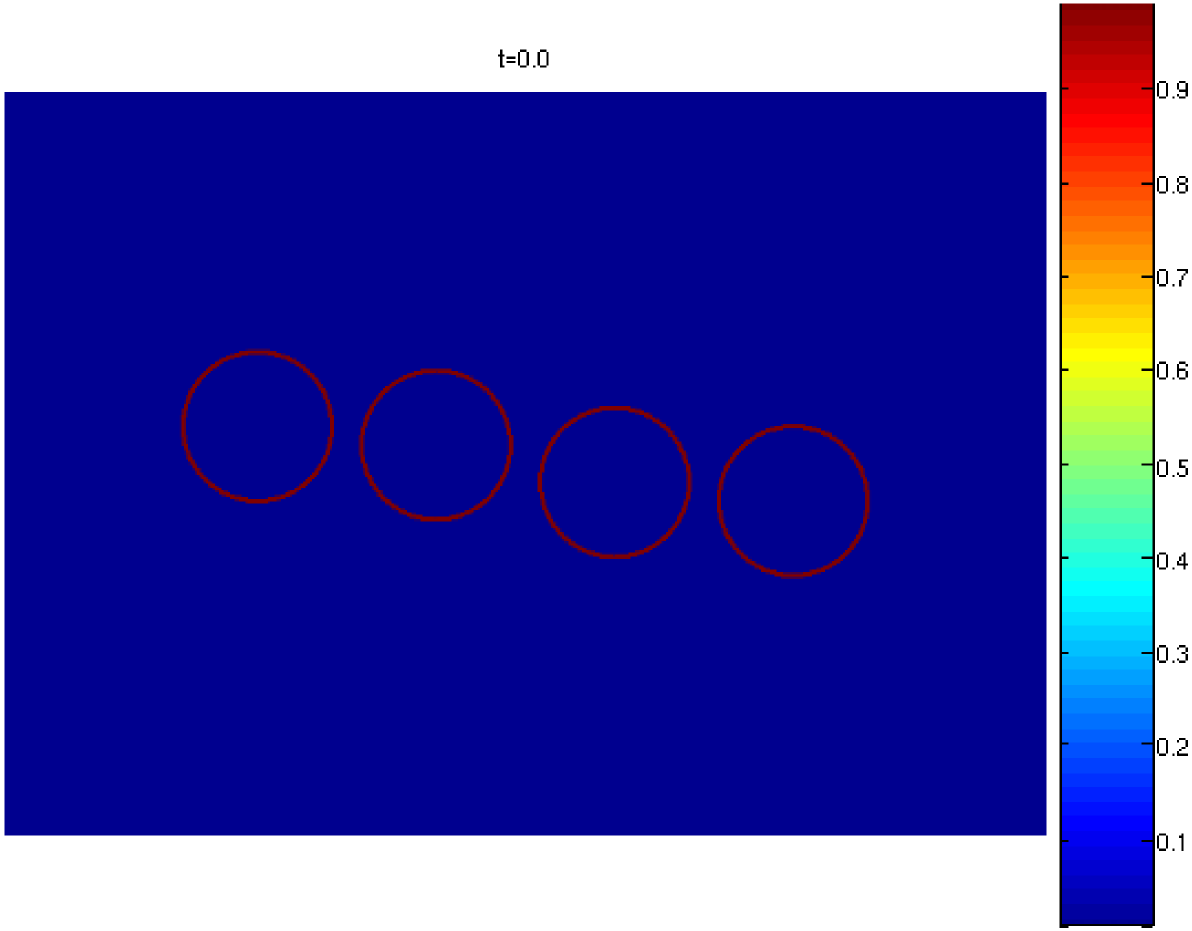

Numerical simulation of cocontinuous polymer blends

Cocontinuous Polymer Blends

Immiscible polymer blends

Intense mixing

3D sponge-like microstructure
Interpenetrating
self-supporting phases

Important route to new materials

(solid materials, tissue scaffolds)

Droplet / Matrix morphology

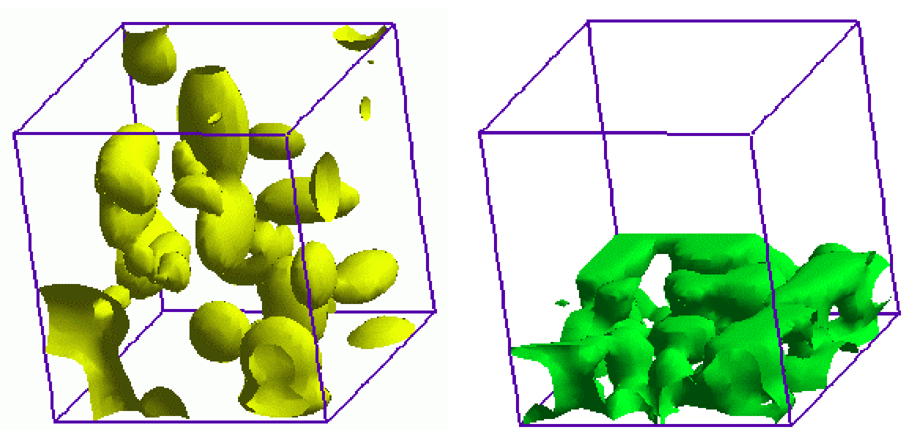

Cocontinuous morphology

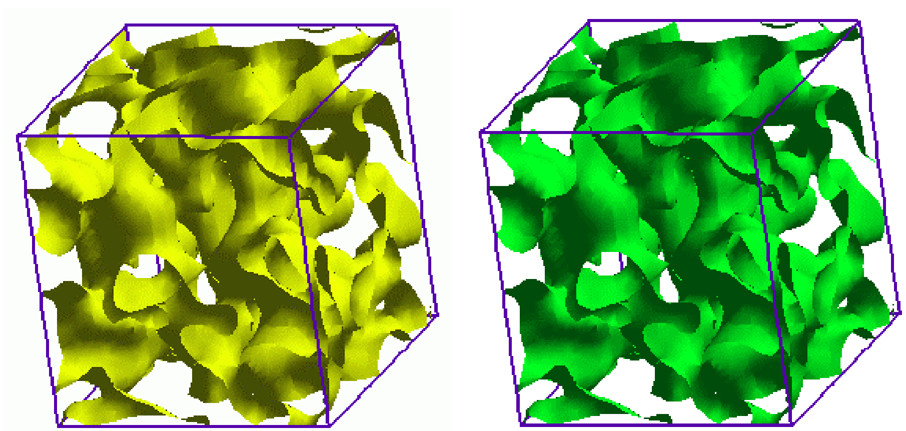

Drops → Continuous phases

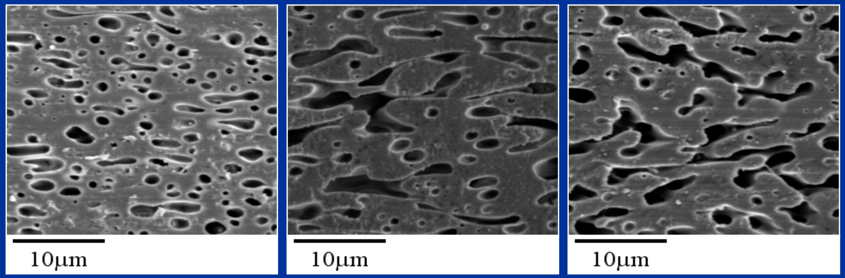

Jeffrey A. Galloway,
Matthew D. Montminy,
Christopher W. Macosko,
Polymer, Vol 43 (2002)

NSF funded collaboration.

- Improved processibility, Static charge control (RTP, B.F. Goodrich) , Packaging for moisture sensitive products (Capitol Specialty Plastics, U.S. Patent 5,911,937), Permeability applications, Tissue scaffolds, Mechanical property improvement

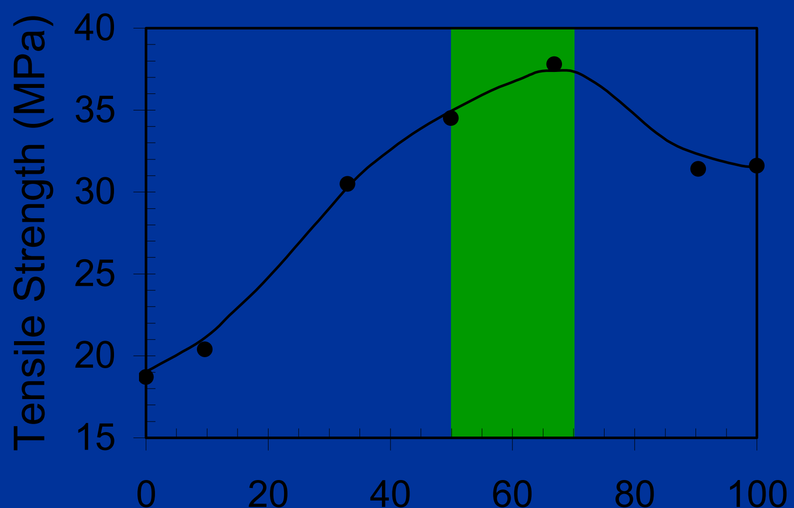

Polypropylene (wt. %)
in Ionomer (Xie, 1991)

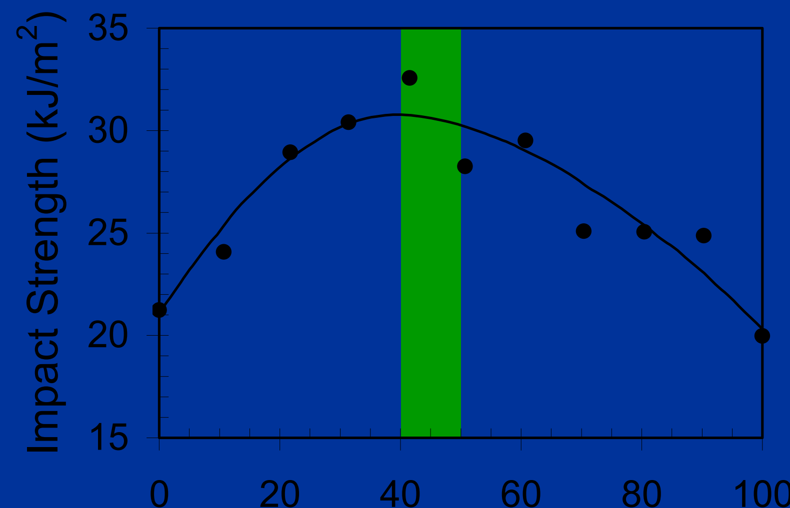

Polyamide 6 (wt. %)
in PVDF (Liu, 1998)

Experiments:

Features of cocontinuous flows

- Fully 3D structures
- Detection difficult
- Optimized control parameters for formation
- Stability of microstructures (non-equilibrium)

- Macroscopic properties depend on microstructure

Theory/numerics:

- Many topology transitions
- Large number of interfaces (complex microstructures)

$\longrightarrow$ Continuum interface methods

Governing equations for single fluid flow

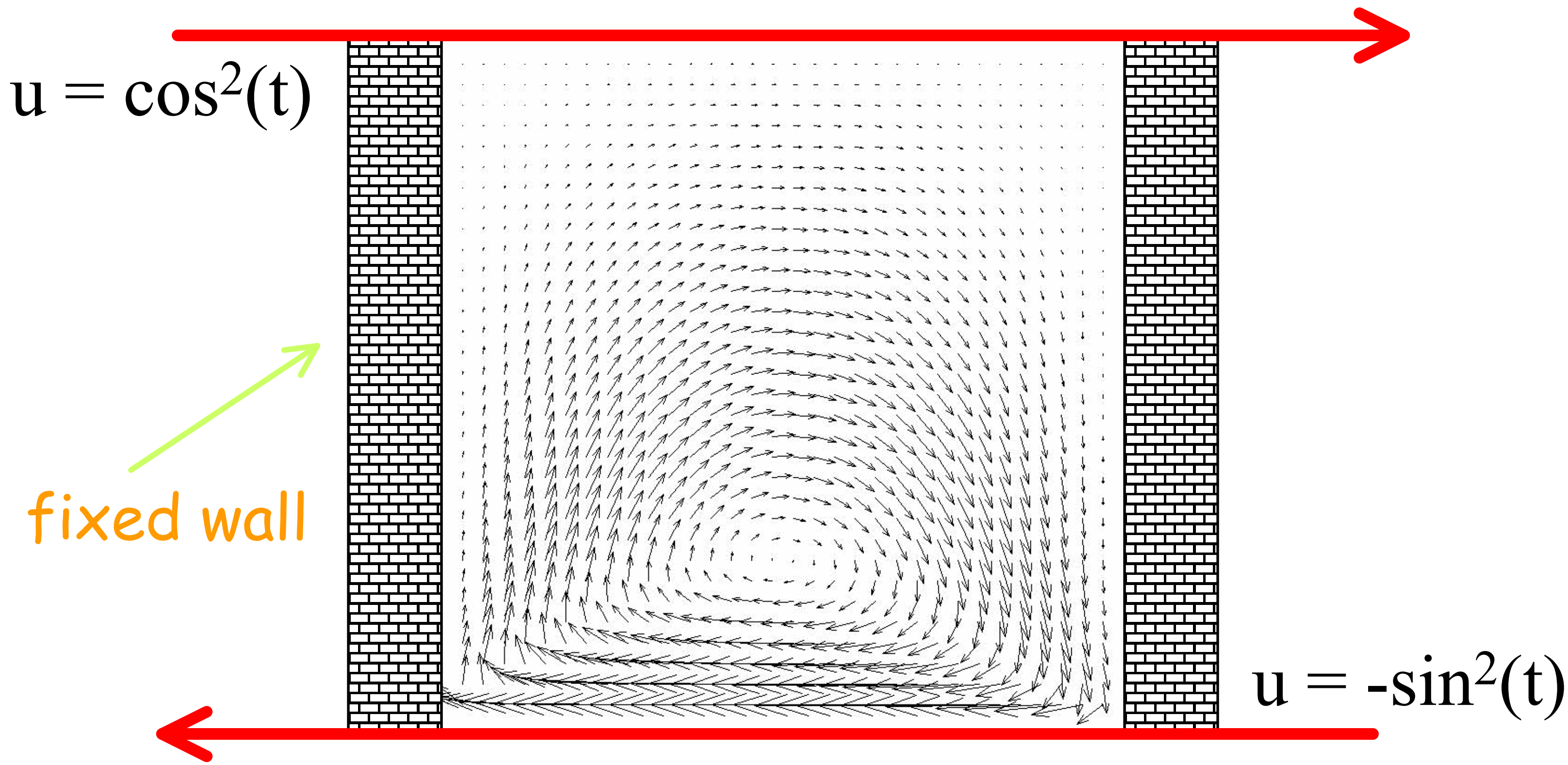

Navier-Stokes equations

$$\rho\left(\frac{\partial \mathbf{u}}{\partial t} + \mathbf{u}\cdot\nabla\mathbf{u}\right) = -\nabla p + \eta\Delta\mathbf{u} + \rho\mathbf{g},$$

$$\nabla\cdot\mathbf{u} = 0$$

Governing equations for multi-fluid flow

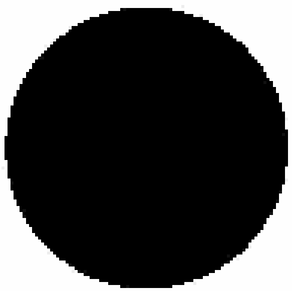

Navier-Stokes equations

$$\boxed{\begin{aligned} \rho_1\left(\frac{\partial \mathbf{u}_1}{\partial t} + \mathbf{u}_1 \cdot \nabla \mathbf{u}_1\right) &= -\nabla p_1 + \eta_1 \Delta \mathbf{u}_1 + \rho_1 \mathbf{g}, \\ \nabla \cdot \mathbf{u}_1 &= 0, \text{ in fluid 1} \end{aligned}}$$

$$\begin{aligned} \rho_2\left(\frac{\partial \mathbf{u}_2}{\partial t} + \mathbf{u}_2 \cdot \nabla \mathbf{u}_2\right) &= -\nabla p_2 + \eta_2 \Delta \mathbf{u}_2 + \rho_2 \mathbf{g}, \\ \nabla \cdot \mathbf{u}_2 &= 0, \text{ in fluid 2.} \end{aligned}$$

Laplace - Young equation

$$[-p\mathbf{I} + \eta(\nabla \mathbf{u} + \nabla \mathbf{u}^T)]_\Gamma \cdot \mathbf{n} = \sigma \kappa \mathbf{n}$$

$$\begin{aligned} \rho\left(\frac{\partial \mathbf{u}}{\partial t} + \mathbf{u} \cdot \nabla \mathbf{u}\right) &= -\nabla p + \eta \Delta \mathbf{u} + \rho \mathbf{g} \boxed{- \sigma \kappa \delta_\Gamma \mathbf{n}}, \\ \nabla \cdot \mathbf{u} &= 0 \end{aligned}$$

Phase-field model

- Multi component,
  multi phase fluid flows
  with deformable interfaces

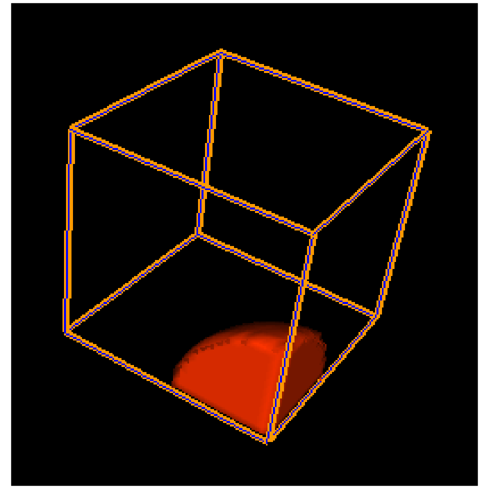

- Topological changes
  (merging, pinch-off)

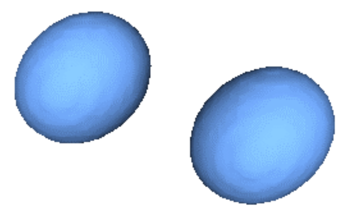

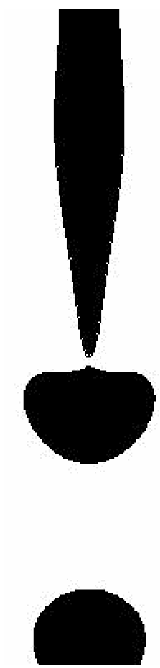

- Increasingly popular method

  Anderson, McFadden, Wheeler, Shen, Liu, Feng, Glasner, Bertozzi,…

Phase-field modeling of multicomponent flows

$$
\begin{aligned}
\nabla \cdot \mathbf{u} &= 0, \\
\mathbf{u}_t + \mathbf{u} \cdot \nabla \mathbf{u} &= -\nabla p + \frac{1}{Re} \nabla \cdot [\eta(c)(\nabla \mathbf{u} + \nabla \mathbf{u}^T)] \\
&\quad - \frac{\epsilon \alpha}{We} \nabla \cdot \left(\frac{\nabla c}{|\nabla c|} \right) |\nabla c| \nabla c, \\
c_t + \mathbf{u} \cdot \nabla c &= \frac{1}{Pe} \nabla \cdot (M(c) \nabla \mu), \\
\mu &= f(c) - C \Delta c,
\end{aligned}
$$

Navier-Stokes-Cahn-Hilliard system

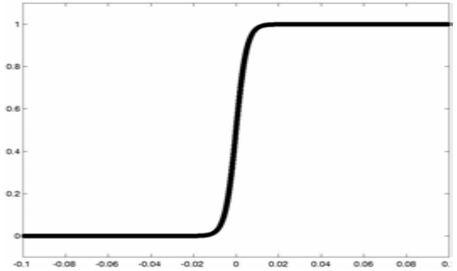

Converges to sharp interface as ε approaches zero:
(Liu & Shen; J. Lowengrub and L. Truskinovsky)

New improvement for phase-field models

Continuum Surface Force)

$$\rho\left(\frac{\partial \mathbf{u}}{\partial t}+\mathbf{u}\cdot\nabla\mathbf{u}\right) = -\nabla p+\eta\Delta\mathbf{u}+\rho\mathbf{g}\boxed{-\sigma\kappa\delta_\Gamma\mathbf{n}},$$

$$\nabla\cdot\mathbf{u} = 0$$

$$\mathbf{F}_1=\sigma\epsilon\alpha\nabla\cdot(|\nabla c|^2 I-\nabla c\otimes\nabla c),$$

$$\mathbf{F}_2=\frac{\sigma\alpha}{\epsilon}\mu\nabla c,$$

$$\mathbf{F}_3=-\frac{\sigma\alpha}{\epsilon}c\nabla\mu,$$

$$\boxed{\mathbf{F}=-\sigma\nabla\cdot\left(\frac{\nabla c}{|\nabla c|}\right)\epsilon\alpha|\nabla c|^2\frac{\nabla c}{|\nabla c|}}$$

J.S. Kim JCP 2005.

Numerical methods

1. Projection method for the Navier-Stokes equation
2. Crank-Nicholson for the Cahn-Hilliard equation, nonlinear multigrid method

$$\frac{\mathbf{u}^{n+1}-\mathbf{u}^{n}}{\Delta t} = -\nabla_d p^{n+\frac{1}{2}} + \frac{1}{2Re}\nabla_d \cdot \eta(c^{n+1})[\nabla_d \mathbf{u}^{n+1} + (\nabla_d \mathbf{u}^{n+1})^T] + \frac{1}{2Re}\nabla_d \cdot \eta(c^{n})[\nabla_d \mathbf{u}^{n} + (\nabla_d \mathbf{u}^{n})^T] + \mathbf{F}^{n+\frac{1}{2}} - (\mathbf{u}\cdot\nabla_d \mathbf{u})^{n+\frac{1}{2}}$$

$$\frac{c^{n+1}-c^{n}}{\Delta t} = \frac{1}{Pe}\nabla_d \cdot [M(c^{n+\frac{1}{2}})\nabla_d \mu^{n+\frac{1}{2}}] - (\mathbf{u}\cdot\nabla_d c)^{n+\frac{1}{2}},$$

$$\mu^{n+\frac{1}{2}} = \frac{1}{2}[f(c^n) + f(c^{n+1})] - \frac{C}{2}\Delta_d(c^n + c^{n+1}),$$

Conservative multigrid method for Cahn-Hilliard fluid, J. Comp. Phys. Kim, Kang, and Lowengrub (2004).

Convergence to sharp interface limit

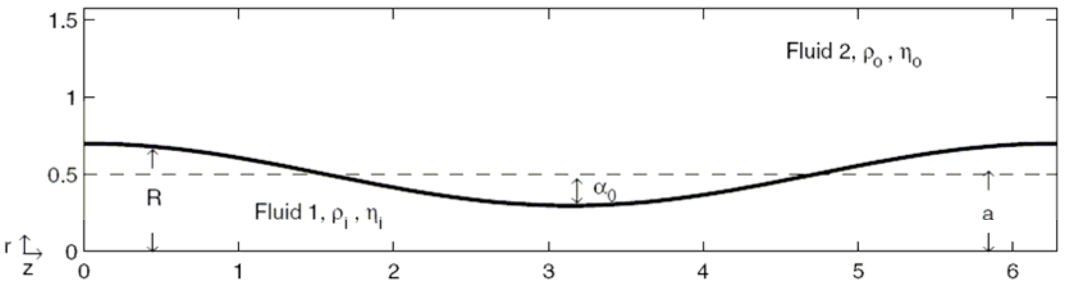

$$R(z,t) = a + \alpha(t)\cos(kz),$$

$\alpha(t) = \alpha_0 e^{int}$, where in is the growth rate

The growth rate is given by linear stability analysis

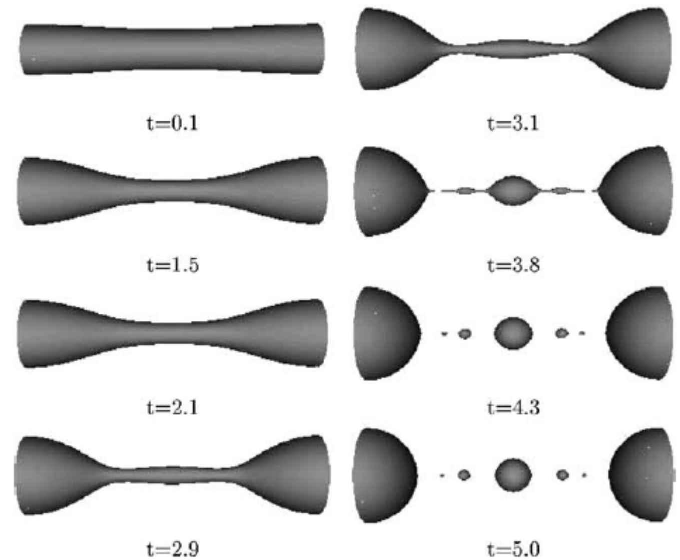

Long time evolution

S. Tomotika, On the instability of a cylindrical thread of a viscous liquid surrounded by another viscous fluid, Proc. Roy. Soc. A 150 (1935) 322–327.

Junseok Kim, A diffuse-interface model for axisymmetric immiscible two-phase flow, Appl. Math. Comput. 160 (2005)

Convergence to sharp interface

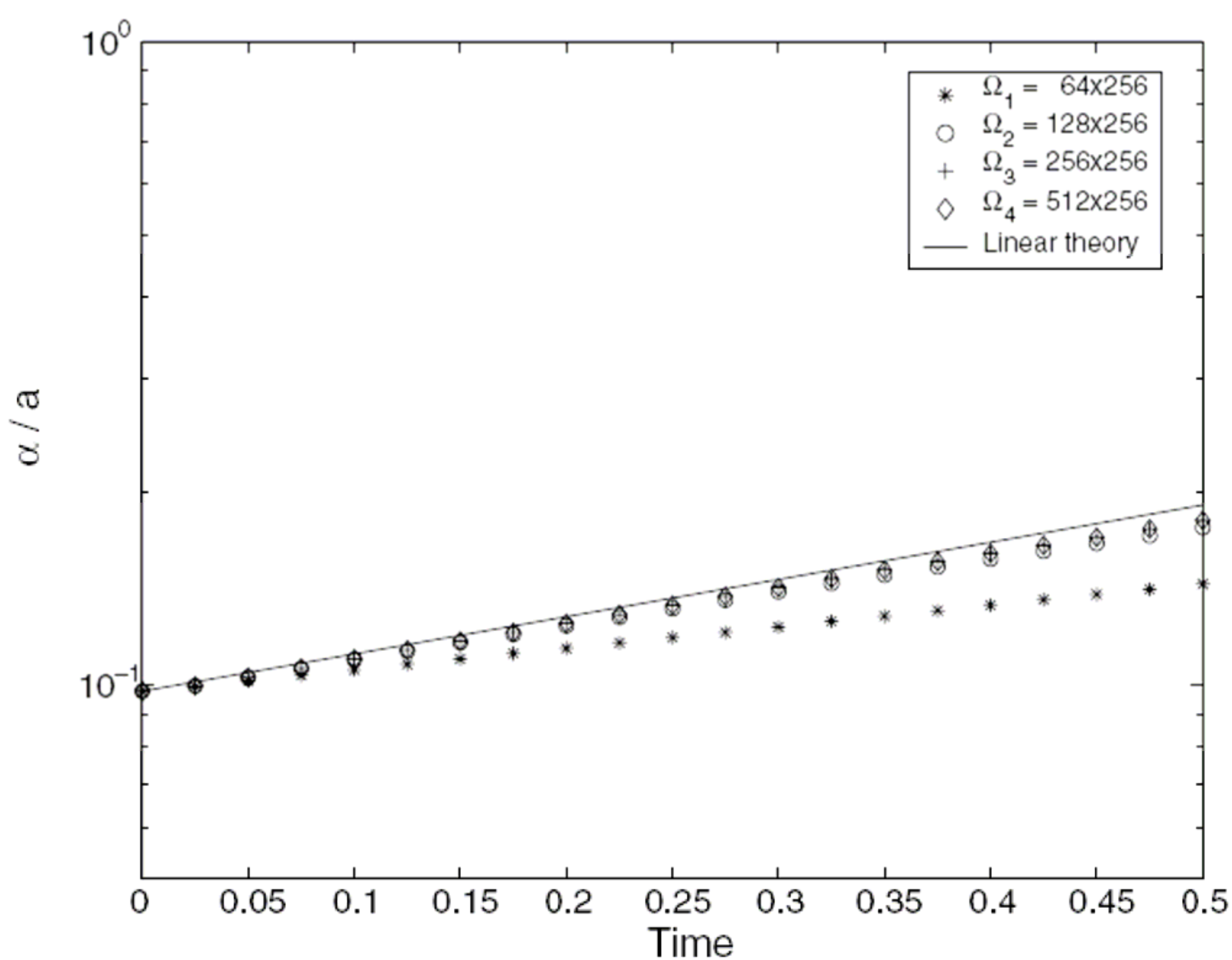

Fig. 4. Evolution of the nondimensional value $\alpha(t)/a$. $\epsilon = 0.02$, $Pe = 100/\epsilon$, $Re = 0.16$, $We = 0.016$. '$*$', '$\bigcirc$', '$+$', and '$\diamondsuit$' are the simulation results on the domains Ω_1, Ω_2, Ω_3, and Ω_4, respectively and the solid line is the linear stability calculation.

Simulation of cocontinuous morphology

Numerical mixing

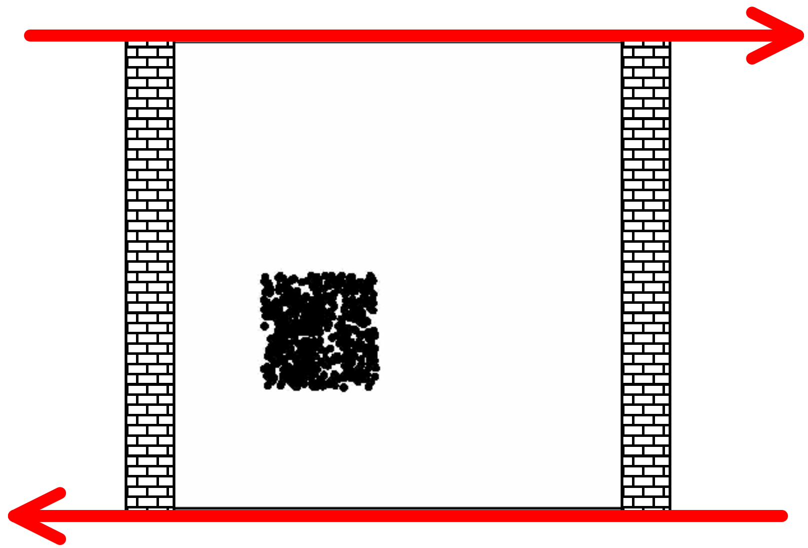

500 massless particles

Ref. J.M. Ottino, The kinematic of mixing: stretching, chaos and transport, Cambridge University Press, 1989.

Interface length / Area

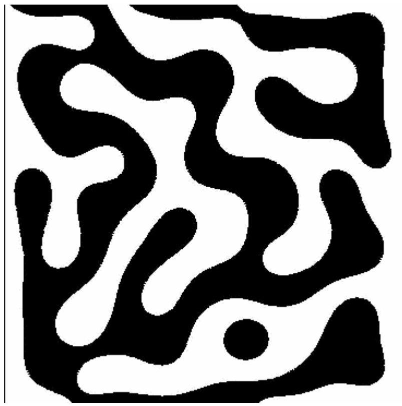

50%

Initial morphology by spinodal decomposition

apply shear flow

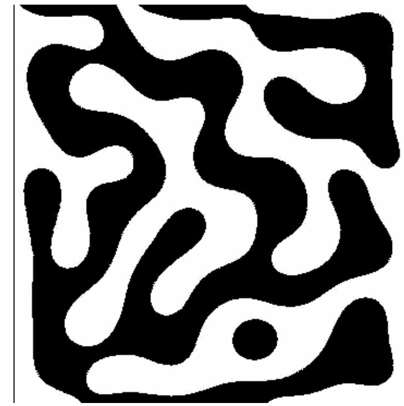

50%

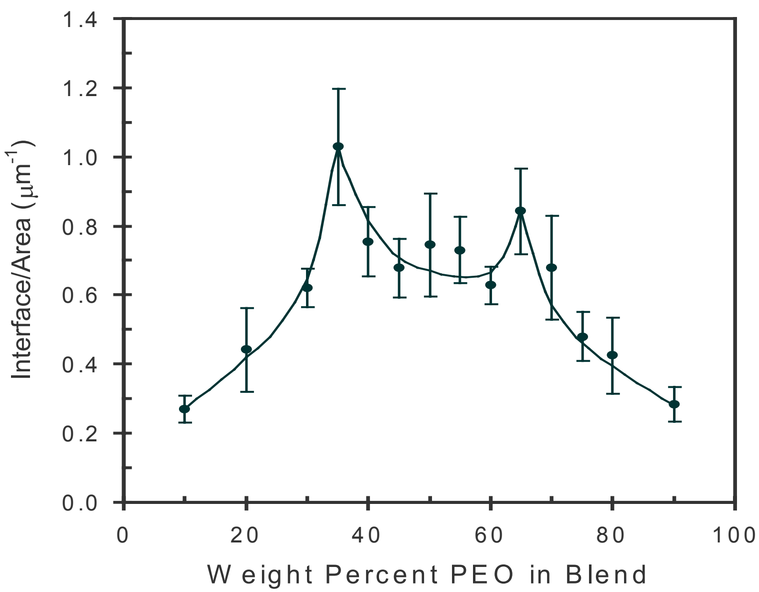

experimental result

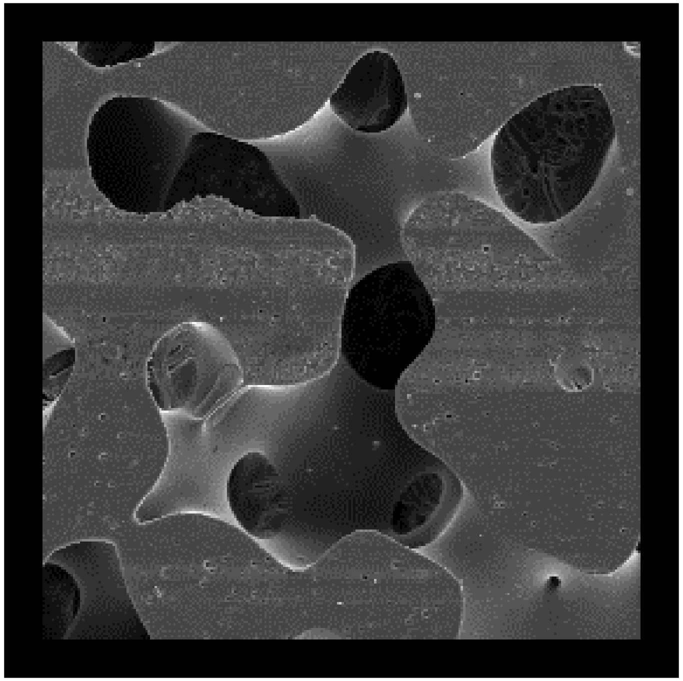

Interface length / Area

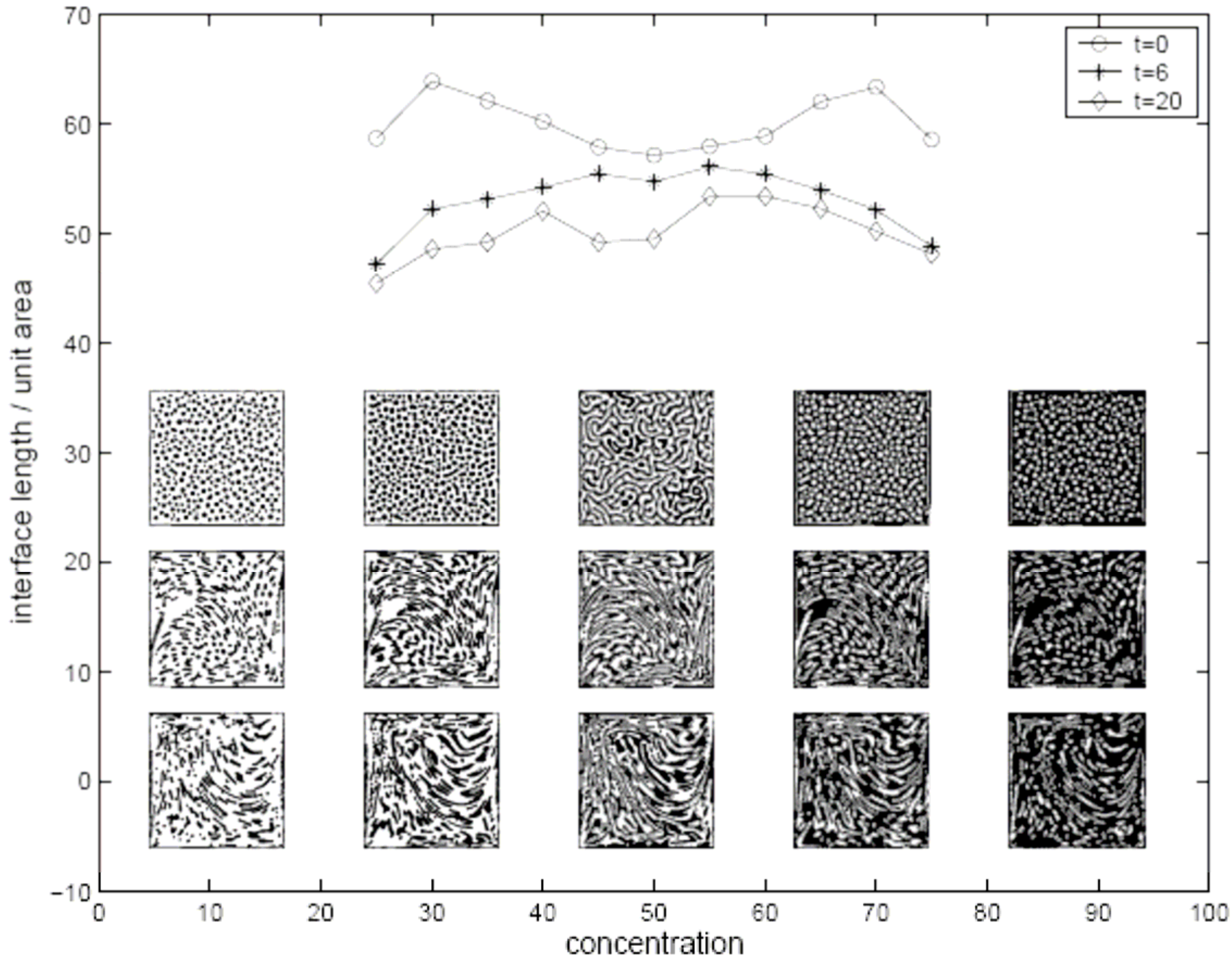

numerical result on 512x512 mesh

Annealing

Scanning electron microscopy

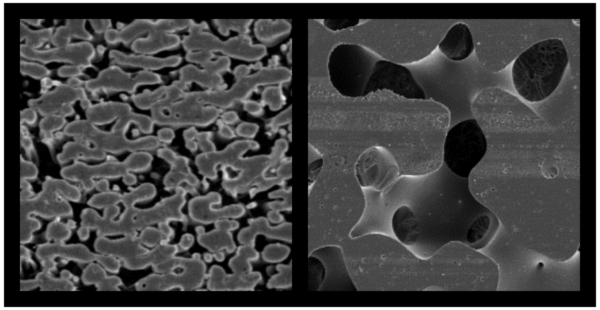

50/50 PEO/PS blend morphology changes dramatically after annealing

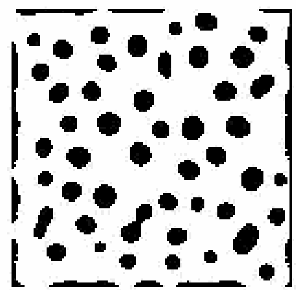

30%

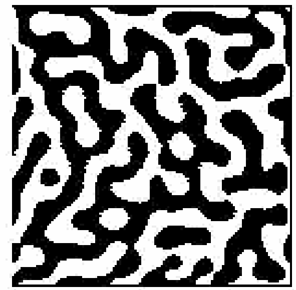

50%

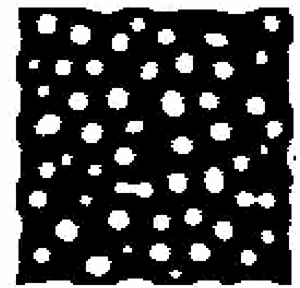

70%

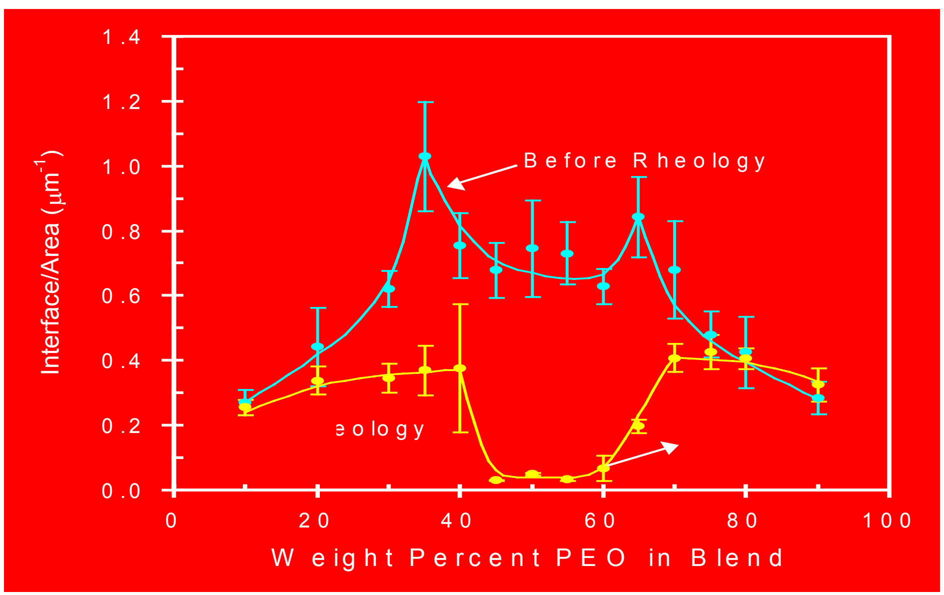

experimental result

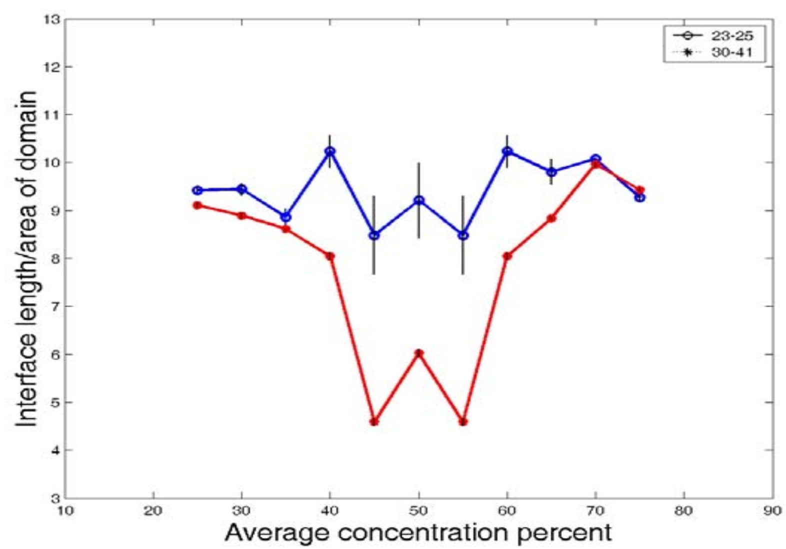

numerical result

3-D simulation

Random shear boundary conditions on top and bottom plates
Periodic boundary conditions on side walls
Randomly distributed ellipsoids.

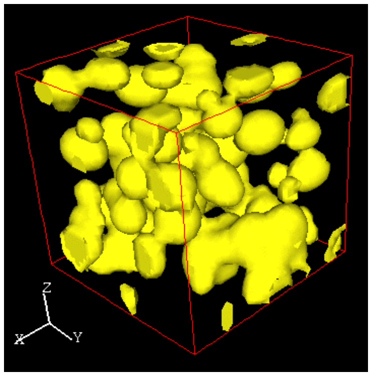

30%

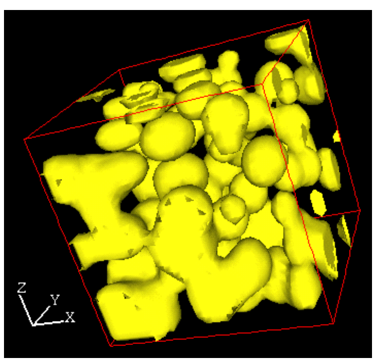

40%

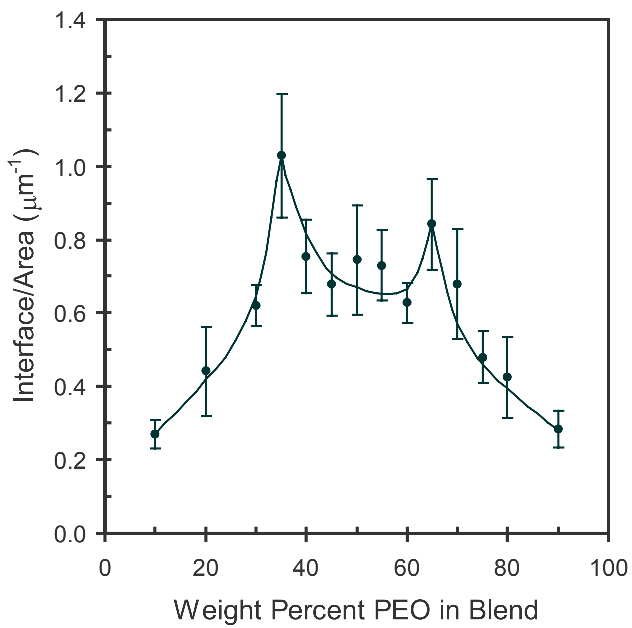

experimental result

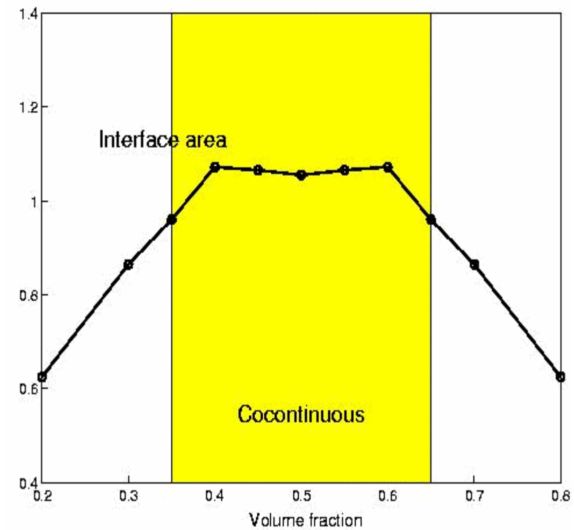

numerical result

Future directions

•Adaptive mesh refinement

Kim, Wise, Lowengrub (in preparation)

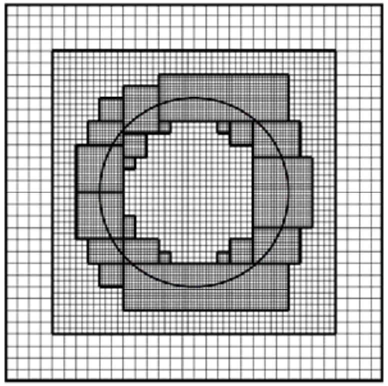

•Complex domains

•Multicomponent (>2) Fluids

Kim, Lowengrub IFB 2005

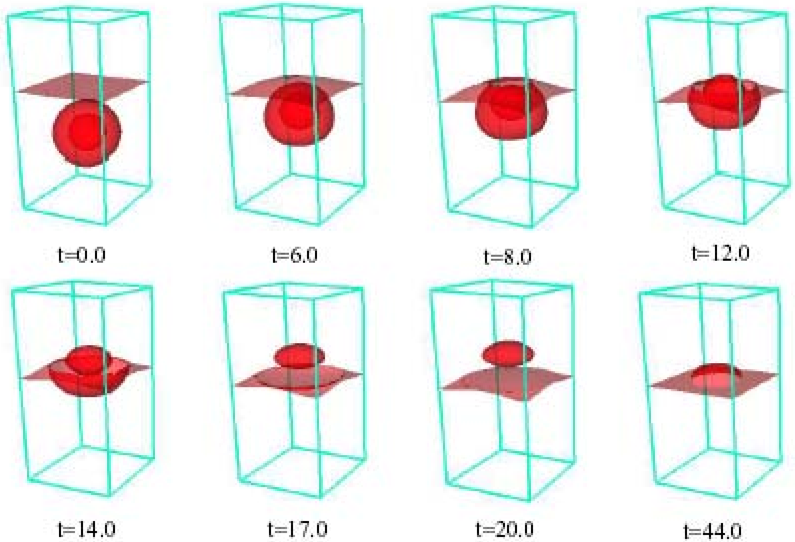

FIG. 4.5. *Evolution of a compound drop, the nondimensional times are shown below each figures.*

•Viscoelastic flow